AIAA Propulsion and Energy Forum
August 24-28, 2020, VIRTUAL EVENT
AIAA Propulsion and Energy 2020 Forum

10.2514/6.2020-3642

Hall2De Simulations of a Magnetic Nozzle

Thomas A. Marks*
University of Michigan, Ann Arbor, MI, 48109

Alejandro Lopez-Ortega † and Ioannis G. Mikellides ‡
Jet Propulsion Laboratory, California Institute of Technology, Pasadena, CA 91109

Benjamin A. Jorns§
University of Michigan, Ann Arbor, MI, 48109

The two-dimensional, fluid-based Hall thruster code Hall2De is adapted to simulate a low temperature propulsive magnetic nozzle. Electron cyclotron resonance (ECR) thrusters developed at the Office National d'Etudes et de Recherches Aérospatiales (ONERA) in France and the University of Michigan are investigated. For each device, the simulated domain is defined from the nozzle throat to a location 10 thruster radii downstream. A numerical mesh is defined based on the measured magnetic field, and the governing fluid equations for singly-charge ions, electrons, and neutrals are solved. The boundary conditions for the throat of the magnetic nozzle are based on measured values of electron temperature and ion velocity. Multiple boundary conditions for the electron temperature in the downstream regions of the domain are considered. The simulated ion velocity and potential agrees well with experiment, while the simulated current densities and therefore thrusts are 50-75% higher than experiment. When a Neumann boundary condition for electron temperature is applied to the far-plume boundaries, the nozzle was seen to be purely isothermal. This suggests that the thermal conductivity along field lines in real devices is much lower than classical simulations predict, and anomalous resistivity may be needed to reproduce the temperature distribution observed in experiment.

I. Nomenclature

k_B	=	Boltzmann constant
$\hat{z}$	=	axial unit vector
$\hat{r}$	=	radial unit vector
$\hat{\theta}$	=	azimuthal unit vector
$\mathbf{E}$	=	electic field vector
ϕ	=	electrostatic potential
$\mathbf{B}$	=	magnetic field vector
n_s	=	Number density of species s
$\mathbf{u}_s$	=	Velocity vector of species s
q_s	=	charge of species s
m_s	=	mass of species s
p_s	=	pressure of species s
T_e	=	electron temperature
$\mathbf{j}_s$	=	current density of species s
Ω_s	=	Hall parameter of species s
ω_{cs}	=	cyclotron frequency of species s

*PhD. Candidate, Department of Aerospace Engineering, Student Member AIAA
†Member of the Technical Staff, Electric Propulsion Group, 4800 Oak Grove Drive, Pasadena, CA, 91109, Mail Stop 125-109, Member AIAA
‡Principal Engineer, Electric Propulsion Group, 4800 Oak Grove Drive, Pasadena, CA, 91109, Mail Stop 125-109, Associate Fellow AIAA
§Assistant Professor, Department of Aerospace Engineering, Senior Member AIAA

II. Introduction

Magnetic nozzle thrusters are a form of of electric propulsion in which the expansion of a heated plasma expands along diverging magnetic field lines generates thrust [1]. The field lines act similarly to the walls of a conventional de Laval nozzle, containing and shaping the plasma as it accelerates to supersonic velocities. However, unlike in those nozzles, the acceleration mechanism is purely electrodeless, and in principle requires no contact between the plasma and any portion of the spacecraft.

This electrodess nature of the acceleration mechanism in magnetic nozzles offers a number of practical advantages. For example, it has the potential to prolong thruster life since the thruster elements are shielded from the types of erosion that more mature technologies with plasma-wetted surfaces such as Hall thrusters and gridded ion thrusters exhibit [2]. Similarly, electrodeless devices like magnetic nozzles theoretically permit the use of more dense but also reactive species such as water and iodine as propellants [3]. This type of capability is highly attractive for missions where propellant storage volume is premium or for enabling future architectures that leverage in situ resource utilization for propellant [4]. Finally, as magnetic nozzles by design are intended to confine the plasma from the thruster walls, these devices in principle may not suffer conventional volume/area scaling laws with size, thereby allowing them to maintain higher overall efficiency at smaller scale. These advantages offered by the magnetic nozzle are particularly enabling for small-spacecraft missions. To this end, there have been multiple efforts to develop this technology to operate in the 10-500 W power range [5, 6].

Despite these on-going efforts, there are a number of unresolved technical challenges for the successful development of magnetic nozzle thrusters. In terms of performance, lower power (< 100 W) devices have historically suffered from low efficiency ($< 11\%$ [7]). More fundamentally, there are also still unresolved questions about the underlying physical processes governing the operation of these devices. The most notable of these is the so-called problem of detachment. As the magnetic field lines which guide the expanding plasma do not terminate and instead circle back to the thruster, the plasma must detach from the field lines in order for the device to generate any thrust. As the ions are unmagnetized, we expect them to follow the plasma potential structure and detach on their own inertia [8]. The question of how the magnetized electrons detach from the field lines is unresolved, and many effects have been proposed to explain this phenomenon, such as electron inertia and non-classical or anomalous resistivity [9]. The manner of detachment is likely to significantly impact the performance of the magnetic nozzle by affecting the divergence efficiency. If the location and manner of plasma detachment could be predicted a priori from the magnetic nozzle's geometry and operating condition, it would dramatically improve the ability of operators to optimize these devices and improve their efficiencies by reducing divergence losses. This would also improve our confidence in their ability to operate on-orbit and perform as expected.

In order to make magnetic nozzles competitive with other EP devices, their design must be improved and optimized and their physics must be better-understood. Additionally, we would like to perform design optimization on these devices, as being able to rapidly alter the operating conditions, geometry, and materials of a thruster in response to data has been key in making huge strides in thruster efficiencies [7]. Kinetic methods, while potentially able to more faithfully capture all of the relevant physics, are too slow to converge in the short timescales between design iterations, so we would like to use a fluid model.

The DIMAGNO model, developed by Ahedo and Merino [1], represents the current state of the art in fully-fluid magnetic nozzle modelling. It has been extensively-used to identify and evaluate possible detachment mechanisms[10]. However, it only considers a fully-ionized, supersonic plasma. Recent experiments have shown that the near-exit-plane region of ECR thrusters may be subsonic[5], and that neutral dynamics may significantly impact the performance of magnetic nozzles[11]. Additionally, DIMAGNO does not include the capability to account for non-classical electron transport, which may dominate classical effects in the thruster plume [12]. To better model these effects, we employ Hall2De, a fluid Hall thruster code developed at the Jet Propulsion Laboratory. Hall2De explicitly considers a partially-ionized plasma and accounts for non-classical transport [13]. These factors make it an ideal candidate for modeling magnetic nozzles. This paper demonstrates the feasibility of modeling a magnetic nozzle using Hall2De and benchmarks its results against data. These benchmarks enable us to gain insight about the physics of magnetic nozzle plasma expansion, and the discrepancies between experiment and data

III. Overview of theoretical questions related to magnetic nozzle operation

In a magnetic nozzle, a plasma consisting of ions and electrons is allowed to expand along diverging magnetic field lines, which are applied by either an array of permanent magnets or by a solenoidal current loop. The less massive electrons are fully magnetized and follow the field lines nearly perfectly, while the ions are heavy and in most devices

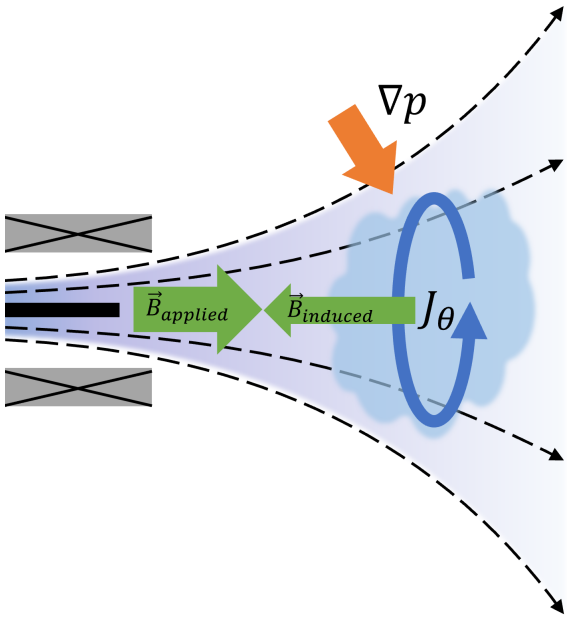

Fig. 1 The operation of a magnetic nozzle

cold and unmagnetized. They proceed on nearly ballistic trajectories but for the electrons, which drag the ions along with them as they expand along the field lines via an ambipolar electric field. The inward-pointing pressure gradient from the vacuum to the denser plasma core creates an azimuthal diamagnetic current [14], which interacts with the applied field via the lorentz force and pushes the plasma downstream. Figure 1 depicts this process on a model magnetic nozzle.

Many aspects of magnetic nozzle performance can be accurately captured with a quasi-one-dimensional model. One-dimensional kinetic models have been very successful in modeling the centerline plasma parameters of magnetic nozzles [5]. However, accurate modeling of the broader two-dimensional structure of the nozzle plasma is needed to deduce the thrust, efficiency, and specific impulse of a given device. To compute these, we need to know the final divergence angle of the nozzle plasma. This is complex and depends on the interaction between the ions and electrons as they expand on different trajectories. Where these trajectories differ from the magnetic field lines, we refer to the plasma as *detached*. Detachment is required for thrust to be produced, as the plasma would otherwise follow the closed field lines back to the spacecraft. This is an inherently two-dimensional processes, so a full picture of magnetic nozzle performance requires a two-dimensional model.

Plasma detachment is a complex topic with a long research history [9, 15]. As ions in a magnetic nozzle are typically unmagnetized, they detach inward from the guiding field lines under their own inertia as they accelerate [16]. The issue of electron detachment is more complex. Since the ions will follow the electrons under an ambipolar electric field, how the electrons detach will impact the trajectories of the ions. Researchers have identified many effects that can cause electron detachment from the field lines, including resistivity [9], electron inertia [6, 10, 15], field line stretching [17], and wave-driven instabilities [12]. There is experimental evidence supporting the presence of all of these effects in at least some magnetic nozzles, so detachment is likely to result from a combination of these effects.

Another open question in magnetic nozzle physics is electron cooling. Polytropic laws of the form $T_e \sim n_e^{\gamma-1}$, where T_e is the electron temperature, n_e is the electron number density, and γ is the polytropic index, have often been applied to magnetic nozzles[16]. Some nozzles do seem to exhibit polytropic cooling [18], while others exhibit more complex behavior [5]. There is a significant gap in our knowledge in our theoretical knowledge of how electrons cool in a magnetically-expanding plasma. In particular, it seems that collisionless cooling alone is insufficient to explain the field-aligned temperature structure and accurately predict the polytropic index of a magnetic nozzle [18]. Instead of prescribing polytropic cooling with an experimentally-derived polytropic index, it would be preferable to solve the full fluid electron energy equation in order to model electron cooling as accurately as possible within a fluid framework.

Neutral dynamics have recently been shown to play a critical role in governing the performance of a magnetic nozzle.

Wachs [11] found that increasing the chamber background pressure significantly decreased the velocity that ions were able to attain, an effect attributed to inelastic electron-neutral collisions. This means that ground tests may be insufficient predictors of in-space performance, and that existing magnetic nozzles which do not model neutral interactions may not be able to reproduce ground test data where background pressures are significant.

In light of the above open questions, we can motivate key capabilities we would want from a model of the thruster

- A robust model of neutral interactions with charged species
- A full electron energy equation
- The ability to incorporate non-classical effects and anomalous resistivity

IV. Methods

A. Overview of Hall2De

Instead of developing a new 2-D fluid plasma code, which would require a significant investment in time and resources, we decided to leverage an existing fluid code - Hall2De [13]. This code, developed at NASA's Jet Propulsion Laboratory, is one of the most extensively-used field-aligned fluid electric propulsion code available. Hall2De was designed to simulate Hall effect thrusters, and its plasma model has been extensively validated against a wide range of experiments, spanning a variety of thruster geometries and operating conditions [13]. It was instrumental in developing the theory behind magnetic shielding [19], and has even been used to simulate high-power nested-channel Hall thrusters [20].

Hall2De treats centrally-mounted cathodes as axisymmetric plasma sources with diverging magnetic field lines - in effect magnetic nozzles. It should thus be possible to simulate a propulsive magnetic nozzle in Hall2De with very few modifications. The densities, magnetic field strengths, and electron temperatures are similar between Hall thrusters and ECR thrusters, with plasma densities of order $10^{14} - 10^{18}$, electron temperatures between 5 and 50 eV, and magnetic fields of a few hundred to a few thousand Gauss [5]. Using Hall2De would have the advantage of including many of the physics that other authors have found to be important in determining the structure of a magnetic nozzle plasma, namely resistivity and electron thermodynamics, without additional work. It could also include many physics which existing magnetic nozzle models neglect, but which could well be important [11], such as interactions with neutral particles, ionization, and higher ion charge states.

In this work, we employ Hall2De for the first time to simulate two existing thrusters. The first of these thrusters is the ECR device designed and built by the Office National d'Etudes et de Recherches Aérospatiales (ONERA) in France. This thruster represents the state of the art in low-power ECR thruster design and has achieved total efficiencies of greater than 10% [7]. The second is the University of Michigan (UM)'s ECR thruster, which is based on the ONERA design, and for which two-dimensional maps of plasma parameters are available [12].

Hall2De's code structure, numerics, and solution procedure have been described in depth in Refs. [13] and [19]. Many modifications have been made to the code since then, but the core plasma model has remained the same. In brief, Hall2De solves the two-dimensional axisymmetric fluid plasma equations on a magnetic field-aligned mesh (MFAM). Hall2De supports up to four ion charge states and four ion fluids of different energy levels per charge state. For each combination of ion fluid and charge state, the ion continuity and momentum equations are solved:

$$\frac{\partial n_j}{\partial t} + \nabla \cdot \left(n_j \mathbf{u}_j\right) = \dot{n}_j \tag{1}$$

$$\frac{\partial n_j \mathbf{u}_j}{\partial t} + \nabla \cdot \left(n_j \mathbf{u}_j \mathbf{u}_j\right) = -\frac{q_j n_j}{m_j}\nabla\phi - \frac{\nabla p_j}{m_j} - \sum_{s\neq i} \nu_{js} n_j \left(\mathbf{u}_j - \mathbf{u}_s\right) - m_j \dot{n}_j \mathbf{u}_n. \tag{2}$$

Here, ϕ is the electrostatic potential, and for a given species j, n_j is the species density, $\mathbf{u}_j$ is velocity vector, q_j is the species charge, m_j is the species mass, p_j is the species pressure, $\dot{n}_j$ is the species rate of production due to ionization/recombination, and ν_{is} is the collision frequency between species j and species s. Equation 1 is the ion continuity equation and balances convection and ionization. Equation 2 is the ion momentum equation, which balances convection on the left against electrostatic forces (first term), pressure gradients (seconde term), drag from inter-species collisions (third term) and effective drag due to ionization (fourth term). An ion energy equation may then optionally be solved. In this work, however, we treat the ions as having a constant temperature $T_i = T_{i,0}$ and consider only one ion fluid and charge state.

The electric potential and electron currents are solved using a combination of the generalized Ohm's law (Eq. 3) and current conservation (Eq. 4). In the equations below, $\mathbf{j_e}$ represents the electron current density, $\mathbf{j_i}$ is the total ion current density, η is the total electrical resistivity, η_{ei} is the resistivity due to electron-ion collisions, Ω_e is the electron Hall parameter, or the ratio of the electron cyclotron frequency to the electron collision frequency, and $\hat{\beta}$ is the field-aligned unit vector. Equation 3 is derived by taking an electron momentum equation of the same form as Eq. 2 and neglecting the inertial terms on the left-hand side. This is noteworthy, as electron inertia has been suggested to play an important role in magnetic nozzles![6, 10].

$$\nabla\phi + \eta\mathbf{j}_e + \eta_{ei}\mathbf{j_i} + \eta\Omega_e\mathbf{j_e}\times\hat{\beta} - \frac{\nabla p_e}{q_e n_e} = 0 \tag{3}$$

$$\nabla\cdot(\mathbf{j_e}+\mathbf{j_i}) = 0. \tag{4}$$

To solve for the electric potential, we decompose Eq. 3 into its field-aligned ($\|$) and cross-field ($\perp$) components and invert it to obtain expressions for $j_{e\|}$ and $j_{e\perp}$. We then substitute these into Eq. 4 to eliminate the electron current density and obtain an expression for the potential, which we solve numerically.

Lastly, the electron fluid energy equation is solved to determine T_e (in electron-Volts):

$$\frac{3}{2}q_e n_e\frac{\partial T_e}{\partial t} = \nabla\phi\cdot\mathbf{j_e} + \nabla\cdot\left(\frac{5}{2}T_e\mathbf{j_e} - \mathbf{Q_e}\right) - \frac{3}{2}T_e\nabla\cdot\mathbf{j_e} - \sum_s \Phi_s + Q_e^T. \tag{5}$$

In this equation, $\mathbf{Q_e}$ is the conductive heat flux tensor and Φ_s is the rate of heat transfer between the electrons and heavy species s. We discretize $\mathbf{Q_e}$ along the $\|$ and $\perp$ directions, such that $\mathbf{Q}_{e\|} = -\kappa_e e\ \|\nabla_\| T_e$ and $\mathbf{Q}_{e\perp} = -\kappa_{e\perp}\nabla_\perp T_e$. The electrical resistivity η and thermal conductivity κ_e are computed using formulations derived from Braginskii's closure [21] as:

$$\eta = \frac{m_e\nu_e}{q_e^2 n_e} \tag{6}$$

$$\kappa_e = 3.16\frac{T_e}{\eta} \tag{7}$$

B. Modifications for magnetic nozzle simulation

We summarize the changes that we made to Hall2De to increase its applicability to magnetic nozzles below:

1) We added the ability for users to select a Neumann boundary condition for T_e at the far plume boundaries ($\nabla T_e = 0$).
2) We now allow direct control over the cathode/inlet mass flow rate instead of requiring that the anode mass flow rate and cathode flow fraction be set. Additionally, the cathode mass flow rate may be set in either standard cubic centimeters per minute (sccm) or kg/s.
3) The user may now select between a uniform ion flux profile at the cathode/inlet or a gaussian profile with configurable width.

These options grant the user more control over the conditions at the inlet, which makes it possible to more faithfully recreate experimental conditions.

C. Boundary conditions

For this work, we were interested only in the magnetic nozzle plasma expansion, so the computational domain only covers the region downstream of the plasma source. As such, we did not include walls in any of the simulations, so no sheath boundaries were needed. In Fig. 2, we depict a notional computational domain for a generic ECR thruster, including all relevant boundary conditions. The Flowthru boundary condition denotes the upstream edge of the domain that is in plane with the thruster exit plane. The R_{max} boundary denotes the boundary surface at the outer radial edge of the domain, and Z_{max} denotes the surface and the maximum axial extent of the domain. At these boundaries, we enforce the following conditions:

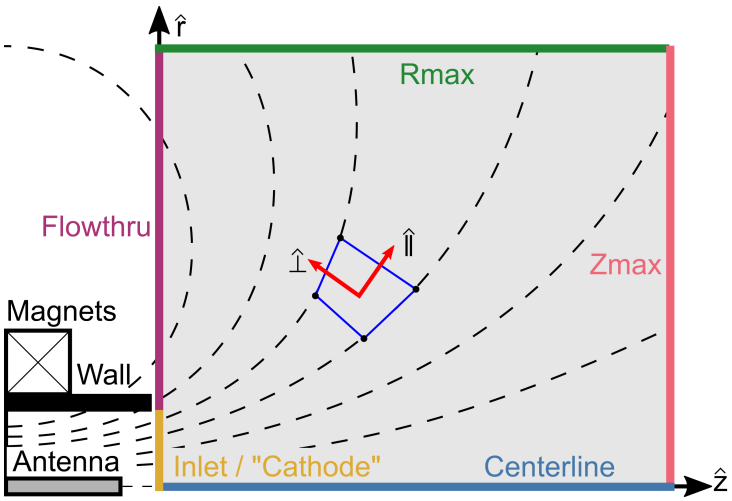

Fig. 2 A generic magnetic nozzle domain and associated boundary conditions. Here, the thruster depicted is an ECR thruster. In blue, we depict a generic mesh element and its associated field-aligned coordinate system.

$$\nabla n_i = 0 \quad \text{for all ion species}$$
$$\mathbf{j_e} + \mathbf{j_i} = 0$$

The first boundary condition is a classical zero-flux supersonic outflow boundary condition, which is appropriate as we expect the plasma to be supersonic over most of the domain. The second boundary current warrants a bit more discussion. In magnetic nozzles, the condition $\mathbf{j}_e = \mathbf{j}_i$ is known as *local current ambipolarity*. This condition is not satisfied over most of the plume and we expect longitudinal currents to develop [1]. *Local* ambipolarity contrasts with *global* ambipolarity, which requires only that $\nabla \cdot \mathbf{j} = 0$, and which is true everywhere in the domain by Eq. 4. Global ambipolarity requires that local ambipolarity be enforced somewhere on the boundary. Ahedo [1] showed that both the inlet and outflow boundaries are natural locations to enforce this condition. We choose the outflow boundary (the combined Flowthru, R_{max} and Z_{max} boundaries) in this work while noting that the inlet may be a more natural choice for magnetic nozzles. Nevertheless, it has been shown that the nozzle plasma is not particularly sensitive to this choice[22].

In addition to the above conditions, the velocity at the Flowthru, Z_{max} and R_{max} boundaries is set such that the flow is forced to exit the domain. This is handled by setting the velocity normal to the boundary to the maximum of the current normal velocity and the ion thermal velocity $v_{th,i}$:

$$\mathbf{u_i} \cdot \hat{n} = \max\left(\mathbf{u_i} \cdot \hat{n}, v_{th,i}\right)$$
$$v_{th,i} = \sqrt{\frac{k_B T_i}{2\pi m_i}}$$

Here, $\hat{n}$ denotes the vector normal to the boundary surface and k_B is the Boltzmann constant. At the inlet, we enforce the following conditions:

$$T_e = T_{e,0} \tag{8}$$

$$\phi = 0 \tag{9}$$

$$c_s = \sqrt{\frac{k_B T_{e,0}}{m_i}} \tag{10}$$

$$\mathbf{u}_i = M_{i,0} c_s \, \hat{z} \tag{11}$$

$$n_i \mathbf{u}_i(r) = \frac{\dot{m}_i}{A_0 m_i} f(r) \, \hat{z} \tag{12}$$

$$f(r) = \frac{\ln a}{1 - 1/a} \exp\left(- \ln a \frac{r^2}{R_0^2} \right) \tag{13}$$

Here, $T_{e,0}$ is a user-defined inlet electron temperature. $M_{i,0}$ is the user-defined ion mach number, c_s is the ion acoustic speed, $\dot{m}_i$ is the mass flow rate of ions, R is the inlet radius, A_0 is the inlet area, and $\hat{z}$ is the axial unit vector. We use Ohm's law to compute the inlet electron current. The ion flux $n_i \mathbf{u}_i$ is purely axial and is determined by a shape function $f(r)$. This function is either 1 for a uniform inlet, or a Gaussian chosen such that $f(0) = \mathrm{a} f(R)$ and such that it gives the same mass flow rate as the uniform case when integrated over the inlet plane. T_{e0} was set such that the simulation and experiment match at first axial location in the data.

D. Electron transport

As discussed in Sec. IV.A, Hall2De treats the electron dynamics with a generalized Ohm's law. By default, the collisionality in the resistivity in this expressions is driven by classical collisions. In our initial trials, we found that when only classical effects are considered, the Hall parameter $\Omega_e = \omega_{ce}/\nu_e$, which is a measure of the relative magnetization of the electrons, is unrealistically large ($\Omega_e > 10^6$) in the region outside of the nozzle, near the Flowthru boundary condition. This is a direct result of the low density and temperatures in this region which give rise to low collision frequency. If left unchecked, this Hall parameter leads to unphysically-large potentials (many millions of Volts) outside of the nozzle-bounding field line, which may disrupt the solution inside of the nozzle by limiting cross-field ion mobility at the nozzle edge. To avoid this artifact, we limit the Hall parameter to 30000 in preserve the stability of the solution within the nozzle. We have found that the the simulation is not sensitive to the value of this upper bound, provided it is significantly larger than the Hall parameter within the nozzle.

E. Mesh, initialization, and convergence

We describe in the following the mesh, inlet conditions, and initialization parameters for the simulations of the two simulated thrusters. As the UM and ONERA thrusters are similar in design, we used the same magnetic field aligned mesh (Fig. 3a) for both simulations. This mesh is based on experimental measurements of the magnetic field in the UM thruster [12]. We do note (Fig. 3b) that there were variations in the centerline magnetic field to that of the ONERA thruster. Minor differences in magnet configuration between the UM thruster and the ONERA thruster lead to small differences in the centerline field profile, but the two are overall very similar.

Table 1 shows the conditions for the simulations we ran. B_0 is the maximum magnetic field, or the magnetic field at $(z, r) = (0, 0)$ and P_b is the background pressure. For the ONERA thruster, we ran two different cases, changing only the boundary condition on T_e. In the first, we set the gradient of the electron temperature at the outflow boundaries (R_{max}, Z_{max},and Flowthru) to zero. In the second, we set T_e at the Z_{max} boundary to an electron temperature, $T_{e,plume}$, based on measurements. We did also run a case where a Neumann boundary condition was applied to the Z_{max} boundary for the UM thruster, but we do not present the results of that simulation here, as they did not demonstrate anything of interest was not present in the first three simulations. We based all inlet parameters for the ONERA thruster on the 2 sccm case at 30 W input power from Ref. [5]. For the UM thruster, we likewise simulated a mass flow rate of 2 sccm and took the inlet electron temperature from Ref. [12]. We also ran The mass utilization efficiency from the 2 sccm case of Ref. [5] (14.2%) was used to set the ratio of ion flux to neutral flux at the inlet for all three cases. Additionally, the number density at the inlet edge was set to a tenth of that on centerline, corresponding to $a = 10$, based on radial measurements of plasma density 30 mm downstream of the exit plane of the UM thruster [12].

We initialize the velocity and potential to zero everywhere in the domain. The electron temperature is initialized to 0.5 eV and the plasma density is set to 10^{12} m$^-$3. The simulation was advanced at a global timestep of around 2×10^-9

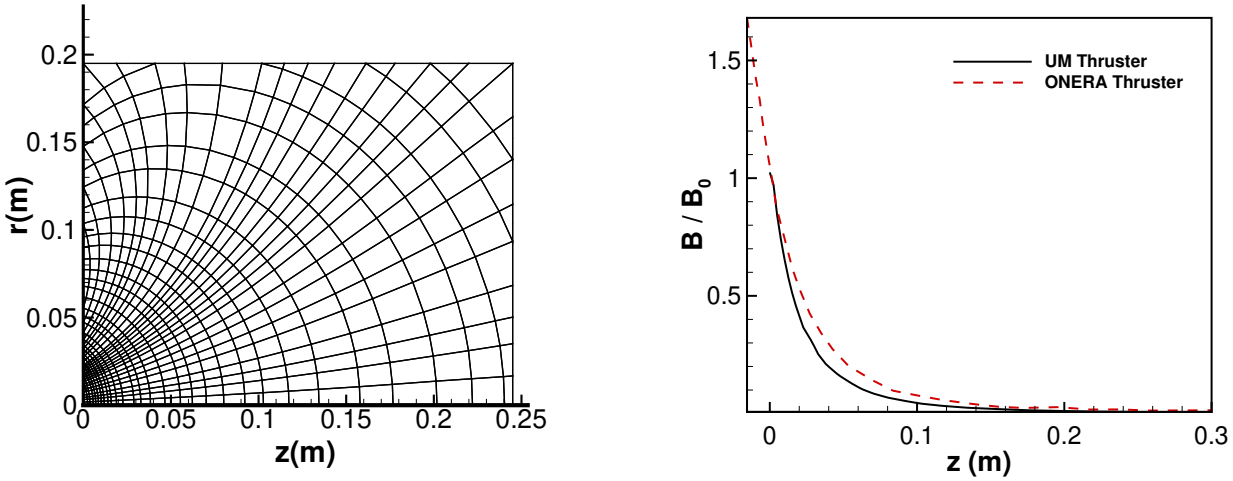

(a) **(b)**

Fig. 3 a) The magnetic field-aligned mesh used in this work based on measurements from the UM ECR thruster. b) Comparison of magnetic field magntiude for the ONERA and UM thrusters relative to B_0, the magnetic field at $z = 0$.

	1. ONERA - Dirichlet T_e	**2. ONERA - Neumann T_e**	**3. UM - Dirichlet T_e**
B_0	550 G	550 G	330 G
$T_{e,0}$	25 eV	25 eV	17 eV
$T_{e,plume}$	15 eV	Neumann	6 eV
$\dot{m}$	2 sccm	2 sccm	2 sccm
$\dot{m}_i/\dot{m}$	0.142	0.142	0.142
$M_{i,0}$	0.43	0.43	0.43
P_b	2.7×10^{-6} Torr	2.7×10^{-6} Torr	4.3×10^{-6} Torr
a	10	10	10

Table 1 Inlet and plume conditions for all three simulations

seconds per iteration, though this number varied depending on the ion Courant numbers. Each case was run for 100,000 iterations, which was more than sufficient to obtain convergence.

V. Results

In this section, we first review the results from the ONERA thruster simulation. We compare our simulation's number density, potential and electron temperature to experimental data for this thruster. As two-dimensional data is not avaialble, we restrict these comparisons to along the thruster centerline. We evaluate the impact of the downstream electron temperature boundary condition on the plasma structure and electron cooling behavior. Then, we compute the thrust and divergence efficiency from our simulation and compare to performance figures from the real device. Next, we compare our UM thruster simulation to two-dimensional number density, potential and electron temperature data.

A. ONERA thruster

We show in Fig. 4 a comparison between the simulation results (cases I and II from Table 1) and experimental measurements from Ref. [5] of the ONERA thruster. As Fig. 4a shows, the Dirichlet electron temperature boundary condition reproduces the experimental profile almost exactly, while the Neumann condition features a slightly steeper potential drop than observed in the experiment, by about 20 V. The number density profile (Fig. 4b is 30-60% higher than the experimental values and is invariant with differences in the plume boundary condition.

Figure 4c compares our simulations' electron temperatures to those measured in [5]. Enforcing a Neumann boundary condition at the R_{max} and Z_{max} boundaries causes the electrons to be isothermal, in contradiction to the data, which show the electrons cooling as the plasma expands. Enforcing a Dirichlet boundary of $T_e = 15$ eV for the electron temperature on the far-plume boundary yields approximately correct magnitudes, though the shape of the cooling curve (Fig. 4d) is different and does not appear to match the polytropic behavior seen in the experiment.

In Figure 5a, we compare the axial velocities between simulation and experiment. Simulation 1 slightly over-predicts the velocity in the near-field, by as much as 10% near to the thruster exit plane, but is almost exactly accurate at larger distances. Simulation 2 predicts velocities about 5% higher than Simulation 1 does in the far field. Figure 5b shows the results of a simulated Faraday probe sweep of 90 degrees at a radius of 0.195 m from the thruster centerline compared to a sweep performed in the experiment at 0.28 m. As the radial extent of the simulation domain is only 0.195 meters, we could not perform an exact copy of the experimental probe sweep, and we expect that the simulated current density will be much larger than the experiment owing to the increase in density the closer one is to the thruster. Thus, to compare the two, we have scaled the simulated results by the $(0.195/0.28)^2$ to approximate the decrease in density with distance. While our simulated profiles barely change between simulations 1 and 2, their magnitudes are two to three times larger than the current densities measured in the experiment. They also feature small off-axis peaks at around 45 degrees, which are also not found in the experiment. Aside from this, the shapes are quite similar, as the divergence efficiency measurements below will quantify.

We can do a direct comparison of performance measurements, efficiency and thrust, from the simulation and experiment as well. In terms of efficiency, we can quantify the effective divergence efficiency, $\eta_D = \cos^2\theta_d$, where θ_d is the divergence angle. This latter parameter can be inferred from measurements of the spatial dependence of the current density (Ref. [23]):

$$\cos\theta_d = \frac{I_z}{I_b} = \frac{\int_{-\pi/2}^{\pi/2} j_i(\theta)\cos\theta|\sin\theta|d\theta}{\int_{-\pi/2}^{\pi/2} j_i(\theta)|\sin\theta|d\theta}, \tag{14}$$

where I_b denotes the beam current and I_z denotes the axial current. To determine thrust from the simulation, we integrate the axial momentum flux over the outflow surfaces with the following expression, where R and Z signify the maximum radial and axial coordinate in the simulation domain, respectively:

$$T = 2\pi m_i \left(\int_0^R n_i u_{iz}^2 r dr + R \int_0^Z n_i u_{iz} u_{ir} dz \right), \tag{15}$$

where T is the thrust and u_{iz} denotes the axial ion velocity. The specific impulse I_{sp} and total efficiency η_T are computed

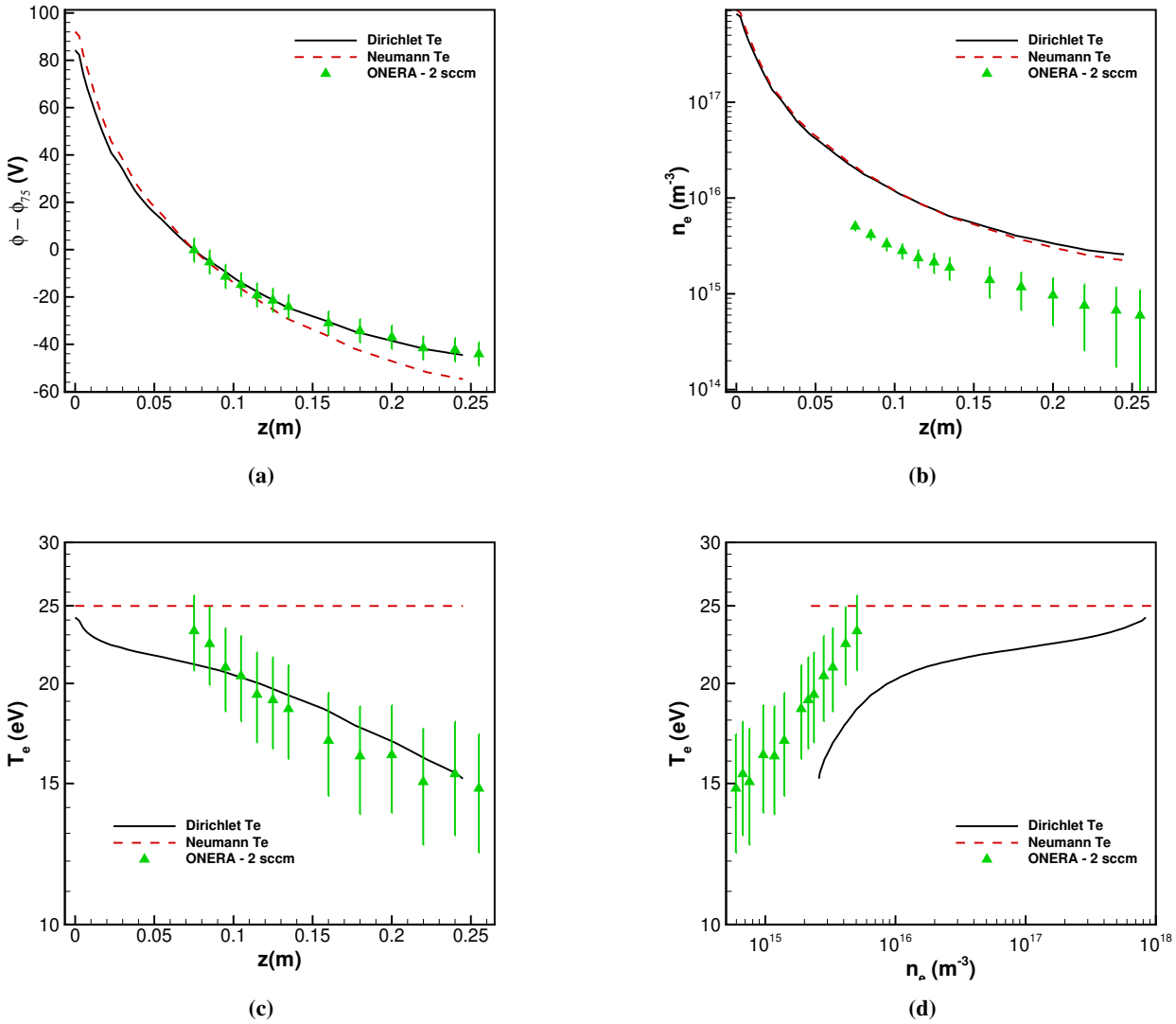

Fig. 4 a) Plasma potential along thruster centerline with respect to the potential at z = 75 mm, b) Plasma density along centerline, c) Electron temperature along centerline, d) Relationship between n_e and T_e

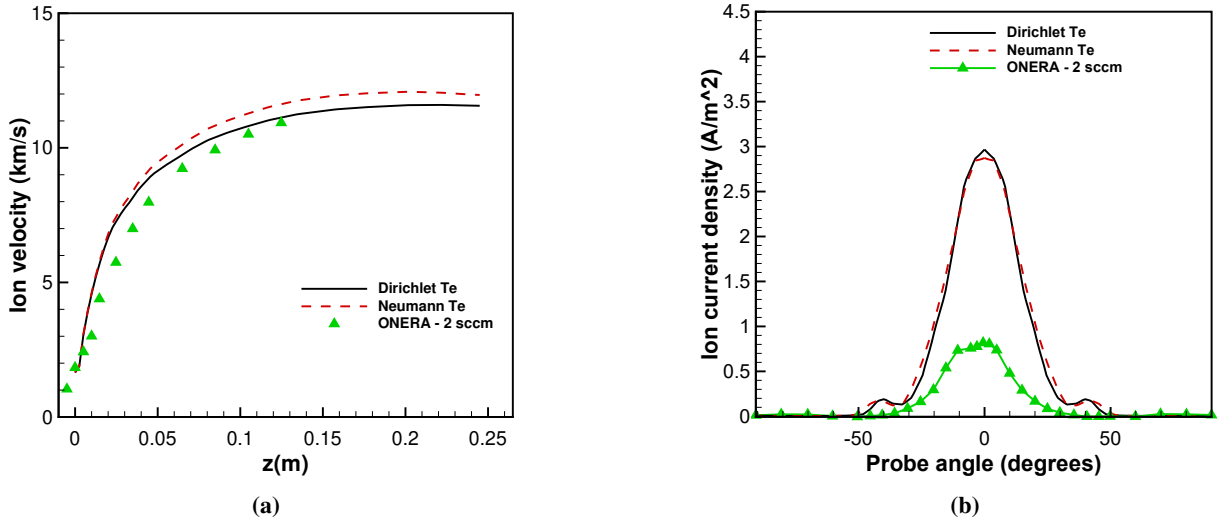

Fig. 5 a) Centerline velocity b) azimuthal sweep of current density

Case	η_d	T	I_{sp}	η_T
Simulation 1 - Dirichlet T_e	84.3%	1280 μN	662 s	13.8%
Simulation 2 - Neumann T_e	83.6%	1470 μN	761 s	18.3%
Experiment - 2 sccm	88.7%	840 μN	436 s	6.0 %

Table 2 Performance comparisons for the ONERA thruster.

using the following expressions, where $g_0 = 9.81$, P_{in} is the input power of 30 W and $\dot{m}$ is the inlet mass flow rate of 2 sccm:

$$I_{sp} = \frac{T}{\dot{m} g_0} \tag{16}$$

$$\eta_T = \frac{T^2}{2\dot{m} P_{in}} \tag{17}$$

Table 2 compares the simulated divergence efficiencies and thrusts to the experimental values from Refs. [5] and [7], respectively. Ref. [7] does not report a thrust measurement for the ONERA thruster at a flow rate of 2 sccm and input power of 30 W. The closest we have is a thrust measurement of 700 μN at 1.5 sccm and 30 W. To estimate what the experimental thrust at 2 sccm might be, we note that thrust scales with the mass flow rate times the exhaust velocity, that the velocity for the 1.5 sccm case is approximately 10% higher than in the 2 sccm case, and that the efficiencies are very similar. All else held equal, this allows us to estimate that the experimental thrust at 2 sccm would be around 840 μN. As the simulated probe sweep implied, our simulation substantially over-predicts the thrust by 50%, resulting in predicted total efficiencies in excess of even the best results from ONERA [7]. However, the simulated divergence efficiencies are very close to the experimental values, within 5%.

B. University of Michigan thruster

Next, we turn to the University of Michigan ECR thruster (simulation 3). We do not have performance measurements for this thruster, so we will only compare simulated plasma parameters to experiment. In reporting the simulation results for the UM thruster, the domain has been constricted to match the experimental domain, which begins at $z = 30$ mm downstream of the nozzle exit. The region upstream of that was still simulated. Beginning with a comparison of

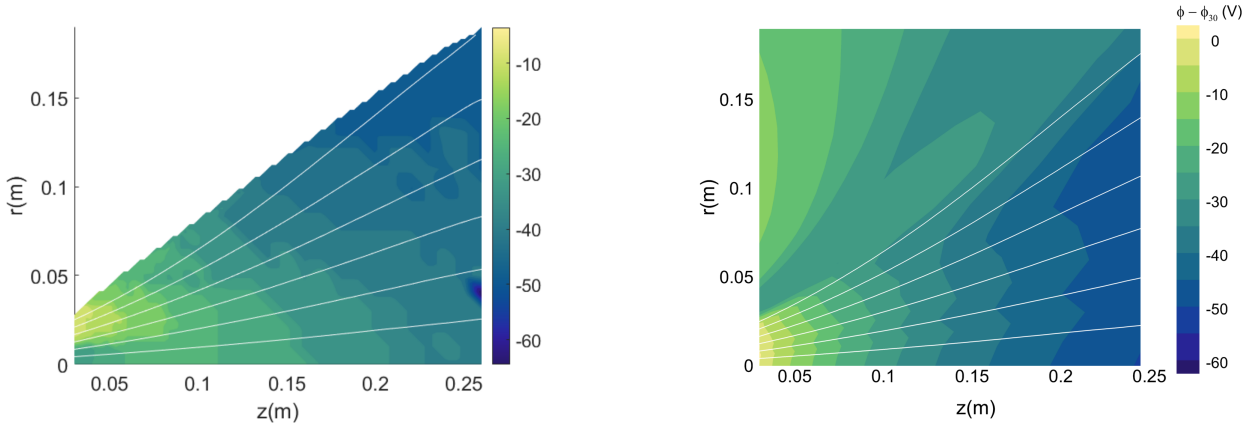

(a) **(b)**

Fig. 6 Comparison of the plasma potential (in Volts) with respect to the potential at $z = 30$ mm between experiment (a) and simulation 3 (b). Magnetic field lines are drawn in white. The simulation domain has been cropped to allow easier comparison

the electric potential and number density (Fig. 6 and Fig. 7), we see some substantial differences with the data. The potential drop is stronger in our simulations than in the experiment by about 10 V. We also fail to reproduce the small centerline potential drop seen on the bottom left corner of Fig. 6a. This structure is likely due to shadowing from the ECR antenna[12], which we do not account for and may explain the discrepancy. The potential contours in Fig. 6a a are also more peaked along centerline and the experimental potential seems to fall off in the radial direction, which does not happen in our simulation within the nozzle. The density (Fig. 7b) is much higher in our simulation than in the experiment by a factor of 5 or more, which we also observed in the ONERA thruster.

Fig. 8 compares the electron temperature between our simulation and the experiment. Given that the plume and inlet electron temperature were simulation inputs, it is unsurprising that the overall trends match well. The experimental data (Fig. 8a) is noisy and has been interpolated, so it is unwise to infer much from the shape of the experimental temperature contours. With that said, our simulation (Fig. 8b) predicts electron temperature contours that are nearly uniform in the cross-field or radial direction near the Z_{max} boundary, which does not appear to be the case in the data. This is likely an artifact of the boundary and not a real feature of electron cooling in a magnetic nozzle

VI. Discussion

A. The role of electron boundary condition

Applying a Dirichlet boundary condition to the plume electron temperature yielded much better agreement with experiment than when a Neumann boundary condition was applied. The Neumann boundary condition resulted in a purely isothermal nozzle, meaning the electron temperature was higher throughout the domain than in the Neumann case. This lead to a potential drop that was nearly 20 Volts lower in the Neumann case than in the Dirichlet case (Fig. 4a) and a velocity at the outflow that was about 500 m/s faster (Fig. 5a), likely due to the stronger potential drop. The choice of electron boundary condition did not significantly alter the centerline number density, thrust, or divergence efficiency.

B. Electron cooling

In Figure 4d, we see that the shape of the curve for the Dirichlet boundary condition case is very different from the linear, near-polytropic cooling seen in the data. Our simulation shows gradually-cooling, near-isothermal behavior ($\gamma \approx 1.1$) at high densties) and rapid, faster-than-adiabatic cooling ($\gamma \approx 1.8$) at low densities, near the Dirichlet boundary condition. This compares to an experimentally-measured value of $\gamma = 1.23 \pm 0.02$ [5], which was approximately constant across all densities. However, as the temperature was fixed on either end of the domain, the electrons were

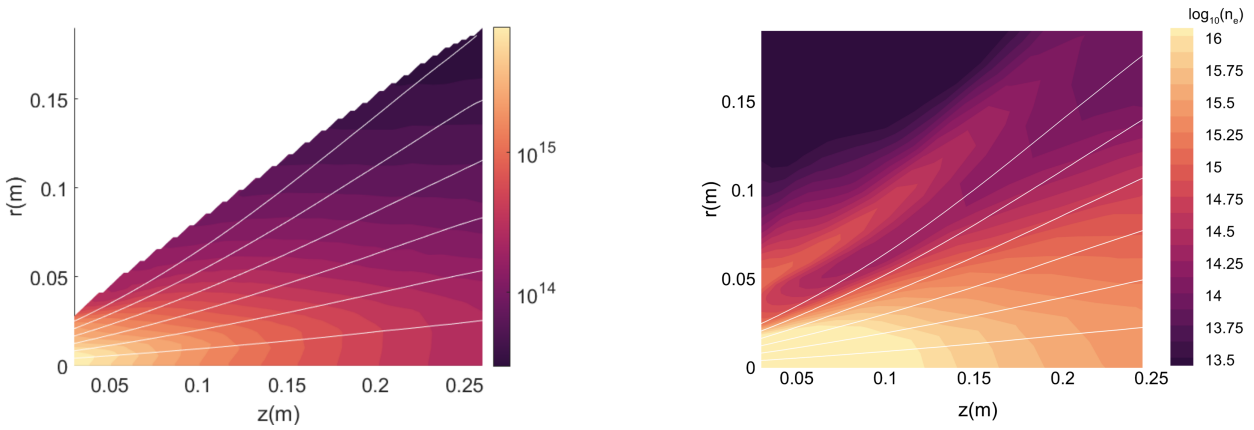

Fig. 7 Plasma density for the experiment (a) and simulation 3 (b). Magnetic field lines are drawn in white. The simulation domain has been cropped to allow easier comparison

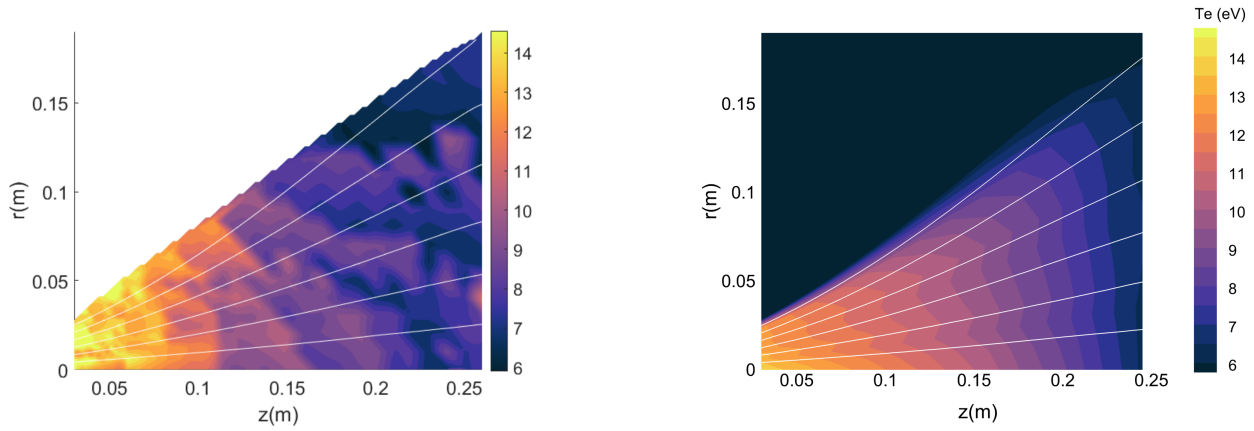

Fig. 8 Electron temperature (eV) in the experiment (a) and in simulation 3 (b). Magnetic field lines are drawn in white. The simulation domain has been cropped to allow easier comparison

forced to cool, so the specific cooling behavior is not representative of the behavior of a real nozzle, in which no such constraint exists.

That we observe a purely isothermal nozzle when the Neumann BC is specified indicates that the thermal conductivity along field lines is far higher than in a real nozzle. This makes sense given our formulation of heat conductivity, which scales with the inverse of the electrical resistivity, which low in the current model of Hall2De, which was developed for Hall thrusters, due to a low classical collision frequency. If resistivity is indeed responsible for electron cooling in magnetic nozzles, our results imply that many more collisions than classical theory predicts may be necessary to reproduce the experimentally-observed cooling behavior.

It has been suggested that kinetic effects may be responsible for polytropic behavior in magnetic nozzles [24]. If such effects cause large deviations from the equilibrium distribution function, then fluid-electron based codes like Hall2De would not be able to accurately capture electron cooling in these thrusters. However, one-dimensional collisionless kinetic models also fail to accurately model the polytropic indices seen in experiment [1, 18]. Our work does not settle the question of electron cooling in a magnetic nozzle, and it is likely both kinetic and resistive effects play important roles.

C. Plasma structures at the nozzle edge

The most interesting features of our simulations are the large off-axis increase in density observed in Fig. 5b and Fig. 7b and the sharp dip and subsequent rise in plasma potential at the edge of the nozzle (Fig. 6b). Neither of these features appear in the experimental data for the UM thruster. However, the density structures bare some resemblance to the "density conics" observed by other authors [25, 26]. Like these authors, we see a density profile which initially peaks near the thruster centerline and then "hollows out" with increasing distance from the exit plane as the on-axis peak decreases in magnitude and the off-axis peak increases. Unlike these authors, however, who show this region of high density emerging along the edge of the nozzle, our density structure seems to exist just outside of it. This is likely related to the second major discrepancy with experiment, the sudden potential drop or "well" at the edge of the nozzle. Similar features to this have also been observed in experiment [6, 25, 26]. Ions at the edge of the beam are accelerated out of the nozzle by the strong radial electric field and into the potential well. At the far end of the well, the potential sharply increases again, the ions slow, and the density increases (though such potential structures have been observed without corresponding increases in off-axis density [6]). The inward electric field confines the initially-rapid expansion of the ions and focuses the beam.

Our potential well appears significantly steeper than those reported by other authors, with electric fields in the 100 V/cm range on the edge of the nozzle, and somewhat wider (around 0.5 thruster radii). Both of these factors may lead to significant overshoot, as ions are accelerated rapidly to high velocities in the radial direction, and then are free to coast for a relatively long time before being slowed again by the inward electric field on the opposite edge of the well. This likely explains why the peak of our high-density region is further off-axis than other authors report. Introducing more mechanisms for electrons to diffuse radially across the field lines would likely reduce the magnitude of the potential well, which would bring our structure more in line with those observed by other authors, or possibly eliminate it altogether, like we see in the UM experiment. Electron inertia and enhanced resistivity would both have increase the cross-field electron current, and their neglect in this work likely significantly contributes to the formation of these structures.

D. Discrepancies in thrust prediction

The simulated thrusts in Table 2 are somewhat higher than we would expect given the mass flow rate and divergence efficiencies. Multiplying the extrapolated experimental thrust at 2 sccm of 840 μN by the ratio of simulated to experimental divergence efficiencies, we arrive at an expected thrust of 610 μN in Simulation 1 and 590 μN in simulated 2, which are about half of than what we simulate. In Fig. 5b, we see that the current density is a factor of two to theee higher in our simulations than in the experiment. This could suggest that our simulated ion mass flow rate is somehow larger than the experimental ion mass flow rate. To check for this, we integrate the ion flux over the inlet and compare it to what we expect. We find a simulated ion mass flow rate of 0.51 sccm for simulation 1, and 0.58 sccm for simulation 2, as opposed to the value of 0.287 that we would find by multiplying the neutral flow rate of 2 sccm by the measured mass utilization efficiency of 0.142. Both our inlet ion mass flow rate and thrusts are over-predicted by about 50%, so it is likely that this mass flow rate discrepancy explains most of the thrust difference.

One possibility to explain this discrepancy is how we defined mass utilization in our work. We used the experimental results from Ref [7], in which they calculated mass utilization efficiency by integrating the downstream ion flux and dividing by the mass flow rate. However, these estimates were based on downstream measurements whereas we use this

measurement to relate the ion flux at the throat to the mass flow rate in the thruster. As ionization can occur downstream of the thruster exit plane in both real magnetic nozzles and in our simulation, using it as we did may in fact yield an effective overestimate for mass utilization at the inlet plane. To compensate for this effect in future iterations, the mass utilization at the inlet must also be treated as a model parameter to be varied until simulation matches experiment.

E. The need for anomalous resistivity

Several lines of evidence point to the lack of anomalous resistivity in our simulations as the main reason for their discrepancies with experiment. The most significant of these is the isothermal temperature profile we observe when setting a Neumann boundary condition for electron temperature at the far plumes. As this is not observed in real nozzles, this implies that the thermal conductivity along the field lines of a real magnetic nozzle is significantly lower than classical theory predicts. Since the thermal conductivity scales with the inverse of the electrical resistivity, there is likely a significant amount of un-accounted-for resistivity. Hepner [12] showed that instabilities such as the lower hybrid drift instability (LHDI) can increase the effective resistivity in the nozzle plume by a factor of 100. This added resistivity may permit the necessary temperature gradients to develop in the plume such that polytropic behavior can develop. Most polytropic laws used to model electron cooling in magnetic nozzles use an experimentally-derived polytropic index [5, 18], which may "bake in" the effects of instability-induced anomalous resistivity along the magnetic field lines. Many nozzles exhibit cooling behavior which is more complex than a polytropic law [5], which might be recovered with a sufficiently-accurate model for anomalous resistivity.

Anomalous resistivity might improve the simulation in other ways. The region outside of the nozzle near the Flowthru boundary is difficult to treat, owing to low densities and very large Hall parameters. This leads to very strong potential gradients at the edge of the nozzle. As discussed in Section VI.C, by allowing much more electron current across the field lines, anomalous resistivity would smooth these gradients out and increase the density near this boundary. This would increase the physical fidelity of simulations of this region and allow us to make quantitative comparisons with experimental data outside of the nozzle, while eliminating the numerical issues that previously plagued this region.

Our simulations do not currently include azimuthal electron inertia. Electron inertia is very likely to play a role in plasma detachment [6, 10] and would affect the plasma in many of the same ways as anomalous resistivity [9]. Both effects are considered *diffusive* detachment mechanisms, meaning they encourage electron diffusion outward across the field lines. However, a lack of electron inertia cannot explain our temperature profiles, as electron inertia should have no impact on the field-aligned conductivity. Electron inertia is still likely important and probably does enhance cross-field electron current in real nozzles, but only anomalous resistivity can explain the full range of discrepancies we observe.

VII. Conclusion

In this paper, we have simulated a magnetic nozzle with Hall2De. The code was developed to simulate the physics of Hall effect discharges, which exhibit many similarities with those in magnetic nozzles but also bear some distinct differences. In these first Hall2De simulations therefore we have found some significant differences between our results and laboratory measurements. Nevertheless, this work has served as the first critical step toward (1) understanding the factors that govern two-dimensional magnetic nozzle plasma dynamics and (2) identifying the advancements needed in the Hall2De physics models to improve the accuracy of our magnetic nozzle simulations. In particular, it seems evident that the simulation over-predicts the thermal conductivity along field lines, which suggests that some additional resistivity needs to be included. Experiments suggest that anomalous resistivity originating from instabilities such as the lower hybrid drift instability play an important role in magnetic nozzle plasmas, and this work serves as another line of evidence that anomalous resistivity needs to be incorporated to accurately simulate magnetic nozzles in a fluid code.

VIII. Acknowledgements

We would like to thank Shadrach Hepner for providing the magnetic field map and plasma data for the UM thruster, Leanne Su and Austin Brenner for productive conversations, and Ethan Dale for giving feedback on this paper. Part of this research was carried out at the Jet Propulsion Laboratory, California Institute of Technology, under a contract with the National Aeronautics and Space Administration (80NM0018D0004). This work was also supported by an Air Force Office of Scientific Research Young Investigator Program award (FA9550-19-1-0022).

References

[1] Ahedo, E., and Merino, M., "Two-dimensional supersonic plasma acceleration in a magnetic nozzle," *Physics of Plasmas*, Vol. 17, No. 7, 2010. https://doi.org/10.1063/1.3442736.

[2] Vitalievich Loyan, A., and Nikolaevna Khaustova, A., "Hall Thruster Erosion," *Propulsion Systems*, IntechOpen, 2019. https://doi.org/10.5772/intechopen.82654.

[3] Staab, D., Frey, A., Garbayo, A., Shadbolt, L., Fabris, A. L., Gurciullo, A., Grondein, P. E., Moloney, R., Faircloth, D., and Lawrie, S., "Aquajet: an electrodeless ECR water thruster," *2018 Space propulsion conference*, 2018, pp. 14–18.

[4] Dankanich, J. W., and Schumacher, D. M., "Iodine propulsion advantages for low cost mission applications and the iodine satellite (ISAT) technology demonstration," Tech. rep., 2015. URL https://ntrs.nasa.gov/search.jsp?R=20150021456.

[5] Correyero, S., Jarrige, J., Packan, D., and Ahedo, E., "Plasma beam characterization along the magnetic nozzle of an ECR thruster," *Plasma Sources Sci. Technol*, Vol. 28, 2019, p. 95004. https://doi.org/10.1088/1361-6595/ab38e1, URL https://doi.org/10.1088/1361-6595/ab38e1.

[6] Little, J. M., and Choueiri, E. Y., "Electron Demagnetization in a Magnetically Expanding Plasma," *Physical Review Letters*, Vol. 123, No. 14, 2019. https://doi.org/10.1103/PhysRevLett.123.145001.

[7] Vialis, T., and Jarrige, J., "Direct Thrust Measurement of an Electron Cyclotron Resonance Plasma Thruster," 2018. https://doi.org/10.2514/1.B37036, URL www.aiaa.org/randp.

[8] Merino, M., and Ahedo, E., "Plasma detachment in a propulsive magnetic nozzle via ion demagnetization," *Plasma Sources Sci. Technol*, Vol. 23, No. 3, 2014, p. 32001. https://doi.org/10.1088/0963-0252/23/3/032001, URL https://iopscience.iop.org/article/10.1088/0963-0252/23/3/032001https://iopscience.iop.org/article/10.1088/0963-0252/23/3/032001/meta.

[9] Ahedo, E., and Merino, M., "On plasma detachment in propulsive magnetic nozzles," *Physics of Plasmas*, Vol. 18, No. 5, 2011. https://doi.org/10.1063/1.3589268.

[10] Ahedo, E., and Merino, M., "Two-dimensional plasma expansion in a magnetic nozzle: Separation due to electron inertia," *Physics of Plasmas*, Vol. 19, No. 8, 2012. https://doi.org/10.1063/1.4739791.

[11] Wachs, B., and Jorns, B., "Background pressure effects on ion dynamics in a low-power magnetic nozzle thruster," *Plasma Sources Sci. Technol*, Vol. 29, 2020, p. 45002. https://doi.org/10.1088/1361-6595/ab74b6, URL https://doi.org/10.1088/1361-6595/ab74b6.

[12] Hepner, S., Wachs, B., and Jorns, B., "Wave-driven non-classical electron transport in a low temperature magnetically expanding plasma," *Appl. Phys. Lett*, Vol. 116, 2020, p. 263502. https://doi.org/10.1063/5.0012668, URL https://doi.org/10.1063/5.0012668.

[13] Mikellides, I. G., and Katz, I., "Numerical simulations of Hall-effect plasma accelerators on a magnetic-field-aligned mesh," *Physical Review E*, Vol. 86, No. 4, 2012. https://doi.org/10.1103/PhysRevE.86.046703.

[14] Takahashi, K., Chiba, A., Komuro, A., and Ando, A., "Experimental identification of an azimuthal current in a magnetic nozzle of a radiofrequency plasma thruster," *Plasma Sources Science and Technology*, Vol. 25, No. 5, 2016, p. 055011. https://doi.org/10.1088/0963-0252/25/5/055011.

[15] Hooper, E. B., "Plasma detachment from a magnetic nozzle," *Journal of Propulsion and Power*, Vol. 9, No. 5, 1993, pp. 757–763. https://doi.org/10.2514/3.23686.

[16] Merino, M., and Ahedo, E., "Influence of electron and ion thermodynamics on the magnetic nozzle plasma expansion," *IEEE Transactions on Plasma Science*, 2015. https://doi.org/10.1109/TPS.2014.2316020.

[17] Takahashi, Kazunori, Ando, A., "Laboratory Observation of a Plasma-Flow-State Transition from Diverging to Stretching a Magnetic Nozzle," *Physical Review Letters*, Vol. 118, No. 22, 2017, p. 225002. https://doi.org/10.1103/PhysRevLett.118.225002.

[18] Little, J. M., and Choueiri, E. Y., "Electron Cooling in a Magnetically Expanding Plasma," *Physical Review Letters*, Vol. 117, No. 22, 2016. https://doi.org/10.1103/PhysRevLett.117.225003.

[19] Mikellides, I. G., Katz, I., Hofer, R. R., and Goebel, D. M., "Magnetic shielding of a laboratory Hall thruster. I. Theory and validation," *Journal of Applied Physics*, Vol. 115, No. 4, 2014, p. 043303. https://doi.org/10.1063/1.4862313, URL http://aip.scitation.org/doi/10.1063/1.4862313.

[20] Mikellides, I. G., and Lopez Ortega, A., "2D (r–z) numerical simulations of the plasma and channel erosion in a 100 kW class nested Hall thruster," *Plasma Sources Sci. Technol*, Vol. 27, No. 7, 2018, p. 75001. https://doi.org/10.1088/1361-6595/aacacb, URL https://doi.org/10.1088/1361-6595/aacacb.

[21] Braginskii, S. I., "Transport Processes in a Plasma," *RvPP*, Vol. 1, 1965, p. 205. URL https://ui.adsabs.harvard.edu/abs/1965RvPP....1..205B/abstract.

[22] Zhou, J., Pérez-Grande, D., Fajardo, P., and Ahedo, E., "Numerical treatment of a magnetized electron fluid model within an electromagnetic plasma thruster simulation code," *Plasma Sources Science and Technology*, Vol. 28, No. 11, 2019, p. 115004. https://doi.org/10.1088/1361-6595/ab4bd3.

[23] Brown, D. L., Larson, C. W., Beal, B. E., and Gallimore, A. D., "Methodology and Historical Perspectiveof a Hall Thruster Efficiency Analysis," *Journal of Propulsion and Power*, Vol. 25, No. 6, 2020. https://doi.org/10.2514/1.38092.

[24] Martinez-Sanchez, M., Navarro-Cavallé, J., Ahedo, E., and Navarro-Cavall, J., "Electron cooling and finite potential drop in a magnetized plasma expansion," *Phys. Plasmas*, Vol. 22, 2015, p. 53501. https://doi.org/10.1063/1.4919627, URL https://doi.org/10.1063/1.4919627.

[25] Charles, C., "High density conics in a magnetically expanding helicon plasma," *Appl. Phys. Lett*, Vol. 96, 2010, p. 51502. https://doi.org/10.1063/1.3309668, URL https://doi.org/10.1063/1.3309668.

[26] Saha, S. K., Chowdhury, S., Janaki, M. S., Ghosh, A., Hui, A. K., and Raychaudhuri, S., "Plasma density accumulation on a conical surface for diffusion along a diverging magnetic field," *Phys. Plasmas*, Vol. 21, 2014, p. 43502. https://doi.org/10.1063/1.4870758, URL https://doi.org/10.1063/1.4870758.